J Solid State Electrochem (2011) 15:2675–2681
DOI 10.1007/s10008-010-1261-z

ORIGINAL PAPER

Tuning percolation speed in layer-by-layer assembled polyaniline–nanocellulose composite films

Sara Shariki · Soon Yee Liew · Wim Thielemans · Darren A. Walsh · Charles Y. Cummings · Liza Rassaei · Matthew J. Wasbrough · Karen J. Edler · Michael J. Bonné · Frank Marken

Received: 25 September 2010 / Revised: 24 November 2010 / Accepted: 25 November 2010 / Published online: 11 December 2010

Abstract Polyaniline of low molecular weight (ca. 10 kDa) is combined with cellulose nanofibrils (sisal, 4–5 nm average cross-sectional edge length, with surface sulphate ester groups) in an electrostatic layer-by-layer deposition process to form thin nano-composite films on tin-doped indium oxide (ITO) substrates. AFM analysis suggests a growth in thickness of ca. 4 nm per layer. Stable and strongly adhering films are formed with thickness-dependent coloration. Electrochemical measurements in aqueous H_2SO_4 confirm the presence of two prominent redox waves consistent with polaron and bipolaron formation processes in the polyaniline–nanocellulose composite. Measurements with a polyaniline–nanocellulose film applied across an ITO junction (a 700 nm gap produced by ion beam milling) suggest a jump in electrical conductivity at ca. 0.2 V vs. SCE and a propagation rate (or percolation speed) two orders of magnitude slower compared to that observed in pure polyaniline This effect allows tuning of the propagation rate based on the nanostructure architecture. Film thickness-dependent electro-catalysis is observed for the oxidation of hydroquinone.

S. Shariki · C. Y. Cummings · L. Rassaei · M. J. Wasbrough · K. J. Edler · M. J. Bonné · F. Marken (✉)
Department of Chemistry, University of Bath,
Bath BA2 7AY, UK
e-mail: f.marken@bath.ac.uk

S. Y. Liew · W. Thielemans · D. A. Walsh
School of Chemistry, University of Nottingham,
Nottingham NG7 2RD, UK

S. Y. Liew · W. Thielemans
Faculty of Engineering, Process and Environmental
Research Division, University of Nottingham,
Nottingham NG7 2RD, UK

Keywords Polyaniline · PANI · Percolation · Phase propagation rate · Voltammetry · Cellulose · Nanocrystal · Nanofibril · Layer-by-layer assembly · Junction · Electrochromism · Electrocatalysis

Introduction

Natural materials and in particular cellulose as a precursor for nano-composites are of interest in a wide range of applications [1]. In this report, sisal (consisting of 67% cellulose) is employed as a precursor for sulphate-modified cellulose nanofibrils in conjunction with polyaniline to form an electrochemically active film. Considerable interest in polyaniline composites and their electronic properties [2] is linked to application in novel nanostructures [3], actuators [4], assembly for example with DNA strands [5] and in electrochemical sensors [6]. Reviews on polyaniline chemistry [7, 8] and applications [9] have appeared elsewhere.

Films of polyaniline nano-composites have been obtained for example by direct electro-deposition [10], by Langmuir-Blodgett deposition [11], with polystyrene spheres embedded [12] and by electrostatic layer-by-layer deposition [13]. The mechanism of the polyaniline oxidation has recently been reviewed and discussed by Žic [14]. The fully reduced form (leucoemeraldine, see Fig. 1 for the protonated structure) is initially oxidised to "free" radical cations (or polarons) which can propagate through the polymer film to create an electrically conducting phase. The polarons can couple to bipolarons without free spins (as shown for example by EPR methods [15]). Further oxidation leads to emeraldine and pernigraniline.

Electrically conductive composites of native cellulose and polyaniline have been prepared and investigated for

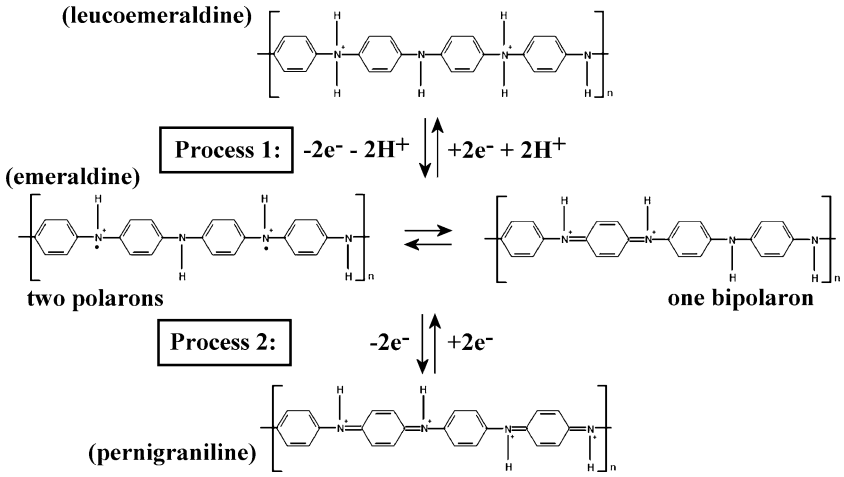

Fig. 1 Simplified mechanism for the switching of redox states in polyaniline in a sulphuric acid environment [14] ignoring anion effects and different states of protonation

acid-treated cellulose precursors [16]. Nanocellulose aerogels have been impregnated with polyaniline to give electrically conducting composites [17] and solution casting methods have been developed for nanocellulose polyaniline composites of variable composition [18, 19]. Co-polymers have been formed by direct electro-deposition with poly-anions [20]. A composite material from cellulose nanofibrils and in situ polymerized aniline was reported to show good electrical properties [21].

Layer-by-layer self-assembly methods have been developed into popular and versatile tools for making very thin membranes and films [22, 23] with controlled thickness. Cellulose has attracted a lot of attention as a versatile sustainable material [24] and as a nano-scale building block [25]. Cellulose "whiskers" have been successfully employed in the electrostatic assembly of a cellulose–cellulose structures [26], cellulose–chitosan structures [27] and cellulose–polypyrrole structures [28], employing other poly-cationic components [29, 30], and with TiO_2 nanoparticles [31]. The layer-by-layer deposition of cellulose nanofibrils with poly-ethoxyaniline [32] has also been reported. Here, sulphate-surface-modified cellulose nanofibrils from sisal are employed to build up films with polyaniline. A low molecular weight (~10 kDa) is shown to give reproducible film deposits with systematic layer-by-layer growth and with well-defined electrochemical properties. The propagation of charges in the nano-composite film is investigated and shown to be nanoarchitecture dependent.

Experimental details

Chemical reagents

Polyaniline (emeraldine base) MW ~ 10,000 Da, *N*,*N*-dimethylacetamide (CHROMASOLV® Plus, for HPLC, ≥99.9%), hydroquinone and H_2SO_4 (95.0–98.0%) were obtained from Sigma-Aldrich. HCl (32%) was obtained from Fisher Scientific. Cellulose nanofibrils 0.69 wt.% solution (4–5 nm average diameter and 250 nm average length nanofibrils derived from sisal with sulphate ester surface functionalities) were prepared by W. Thielemans following an earlier published procedure [33]. Demineralised and filtered water was taken from a Thermo Scientific water purification system (Barnstead Nanopure) with 18.2 MΩcm resistivity. Argon from BOC (Pureshield) was employed to de-aerate solutions. All experiments were performed at T=20±2 °C.

Instrumentation

For voltammetric studies a microAutolab II potentiostat system or a PGSTAT12 bipotentiostat system (EcoChemie, Netherlands) was employed with a Pt gauze counter electrode and a saturated calomel (SCE) reference electrode (Radiometer, Copenhagen). ITO-coated glass (tin-doped indium oxide films, sputter-coated, active area 10×10 mm, resistivity 15 Ω per square) was obtained from Image Optics Components (Basildon, Essex, UK). Cleaning of the ITO surface prior to experimentation was achieved by rinsing with ethanol and water and 30 min heating to 500 °C in an Elite tube furnace in air followed by re-equilibration of the ITO electrodes to ambient conditions for at least 12 h. Atomic force microscopy (AFM) images were obtained using a Digital Instruments Nanoscope IIIa Multimode Scanning Probe Microscope in tapping mode (Veeco TESP probes). SAXS/WAXS (simultaneous small-angle X-ray scattering and wide-angle X-ray scattering) pattern of the electro-deposited cellulose was obtained on a SAXSess system using a PW3830 X-ray generator and the X-ray image plates were observed using a Perkins Elmer Cyclone Storage Phosphor System. Polyaniline–nanocellulose films were

deposited onto ITO-coated polymer for analysis in the diffractometer. A background diffraction pattern for the substrate was subtracted. The patterns with Cu Kα radiation (λ=1.5406) at 40 kV and 50 mA were recorded in the region of 2θ from 0.014° to 5° (0.01 to 28 nm^{-1}) with an exposure time of 10 min.

Layer-by-layer formation of polyaniline–nanocellulose composite films

Solution A Following a literature recipe [34], 200 mg low molecular weight polyanilline was dissolved in 10 cm^3 dimethylacetamide by sonicating for about 8 h [35]. The polyaniline dipping solution was prepared by slowly adding one part (by volume) of the polyaniline solution to nine parts of deionised water that had its pH adjusted to about 3.0–3.5 with HCl. The pH was then quickly lowered to 2.5–2.6 by adding drops of approximately 1 M HCl solution. Care has been taken to not go below a pH of 2.5 or above a pH of 4.0 to avoid precipitation of the polyaniline. The polyaniline dipping solution was stable for several days after preparation.

Solution B The cellulose dipping solution was prepared by adding one part (by volume) of the sisal fibre solution to nine parts of deionised water.

Film formation The clean ITO-coated glass was first dipped into polyaniline solution for 1 min, rinsed with deionised water and then dipped into the cellulose solution for 1 min, followed by rinsing. After each deposition cycle, the sample was dried with a gentle flow of filtered compressed air. The deposition cycle was repeated in order to deposit thicker films. The blue colour of the film is observed to darken with each deposition cycle (see Fig. 2a).

ITO junction electrode preparation and use

Generator–collector experiments were performed at ITO electrodes. Initially, electrodes were patterned by masking off a "U" pattern (Kel-F tape). ITO etching was then carried out in 1 wt.% tartaric acid and 3 wt.% oxalic acid solution at 35 °C for approximately 20 min [36]. The resulting ca. 1 mm wide ITO line (vide infra) was then carefully cut with a focused ion beam (FIB: Ga liquid metal ion source (LMIS), 30 kV, 50 pA ion beam for making a 1 μm deep trench; SEM: Carl Zeiss XB1540) resulting in a ca. 700 nm wide gap or junction (vide infra). Prior to electrochemical experiments these junction electrodes were cleaned (rinsing with water and ethanol, drying, 30 min 500 °C in air and re-equilibration to ambient conditions).

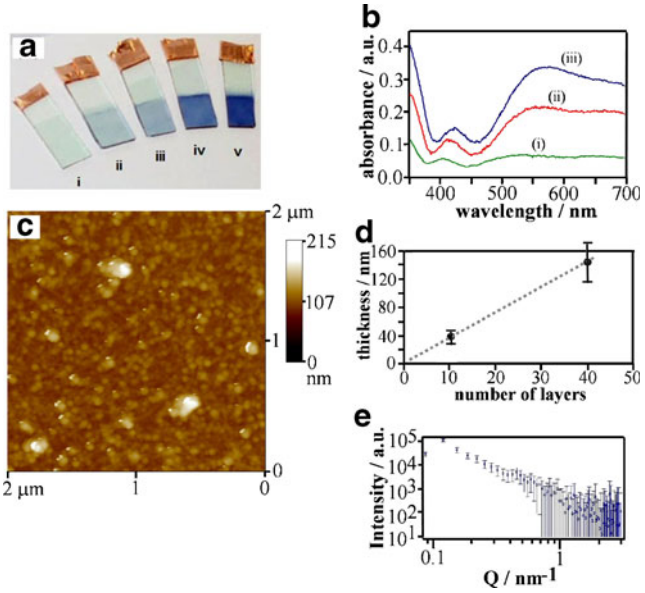

Fig. 2 **a** Photographic image showing a set of polyaniline–nanocellulose coated ITO electrodes with (*i*) 0, (*ii*) two, (*iii*) five, (*iv*) 10 and (*v*) 15 layers. **b** UV-visible spectrum of ITO electrodes with (*i*) two-, (*ii*) 10- and (*iii*) 15-layer polyaniline–nanocellulose film deposits. **c** AFM image showing the surface topography for a 10-layer polyaniline–nanocellulose film with spherical polyaniline and fibrous cellulose clearly visible. **d** Plot of the average film thickness as a function of deposition cycles obtained from AFM images of films with exposed substrate (errors estimated). **e** Small-angle X-ray scattering pattern for a 60-layer deposition of polyaniline–nanocellulose on an ITO-coated polymer film (background subtracted)

Results and discussion

Formation and characterisation of layer-by-layer polyaniline–nanocellulose composite films

Layer-by-layer growth of polyaniline–nanocellulose films can be followed based on the UV/Vis optical absorption. The blue coloration of the films increases visibly with the number of layers (see Fig. 2a) and the resulting UV/Vis spectra are shown in Fig. 2b. Absorption peaks at <350, 430 and 550 nm can be assigned to π–π*, polaron–π* and bipolaron–π* transitions, respectively [37–39], consistent with the emeraldine nature of the commercial precursor.

AFM (tapping mode) images have been obtained to explore topography and to obtain an approximate measure of film thickness. Figure 2c shows a typical topography image with spherical objects of 30–40 nm diameter (coiled polyaniline) and cellulose filaments stretching over several hundred nanometers. Height measurements obtained by scratching the film and exposing the underlying ITO substrate suggest an increase in film thickness of in average 4 nm per layer (very approximate, see Fig. 2d). SAXS data (see Fig. 2e) show a peak at ca. 0.45 nm^{-1}. A Guinier plot (not shown) is consistent with cellulose features of ca.

11 nm average size (radius of gyration) as reported previously [40]. The peak feature suggests some degree of order and a repeat distance in the films of ~14 nm, which matches with the Guinier radius. This repeat distance is likely to be due to a combination of nanocellulose and polyaniline binder.

Electrochemical characterisation of layer-by-layer polyaniline–nanocellulose composite films I.: ion insertion and charge transport

Voltammetry data for polyaniline–nanocellulose films have been recorded in aqueous 0.5 M H_2SO_4. Film deposits on ITO even with only one or two layers of deposit are electrochemically active and exhibit two prominent redox processes (see Fig. 3a). At a midpoint potential of 0.13 V vs. SCE, a chemically reversible voltammetric response with characteristic shape is observed. For a two-layer film deposit the peak currents for oxidation and for reduction change linearly with scan rate (see Fig. 3c). A second chemically reversible voltammetric response is observed with midpoint potential 0.69 V vs. SCE. The two redox processes can be assigned to the initial oxidation of leucoemeraldine to emeraldine (P1, see Fig. 1) and the subsequent oxidation of emeraldine to pernigraniline (P2, see Fig. 1).

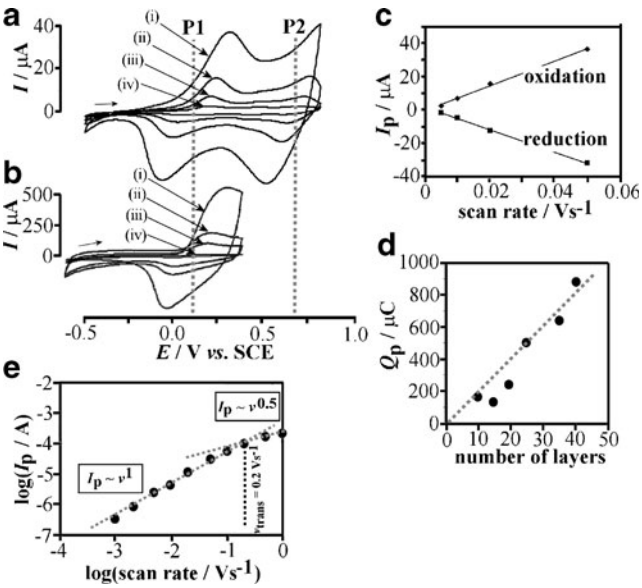

Fig. 3 **a** Cyclic voltammograms (scan rate (*i*) 50, (*ii*) 20, (*iii*) 10 and (*iv*) 5 mVs^{-1}) for a two-layer polyaniline–nanocellulose film on ITO immersed in 0.5 M H_2SO_4. **b** Cyclic voltammograms (scan rate (*i*) 1,000, (*ii*) 200, (*iii*) 100 and (*iv*) 10 mVs^{-1}) for a 40-layer polyaniline–nanocellulose film on ITO immersed in 0.5 M H_2SO_4. **c** Plot of the anodic and cathodic peak currents for process P1 versus scan rate (two-layer film). **d** Plot of the charge under the oxidation peak (scan rate 50 mVs^{-1}) versus number of deposition layers. **e** Plot for the anodic peak current for process P1 versus scan rate (40-layer film)

The number of polyaniline–nanocellulose layers causes a systematic change in the voltammetric response. As the film thickness increases the charge under the oxidation peak, (P1) increases in an approximately linear relationship (see Fig. 3d). When analysed in more detail, a transition in the rate of mass transport can be identified for thicker polyaniline–nanocellulose films. Figure 3e shows a plot of the logarithm or the peak current versus the logarithm of the scan rate with a point of transition (from $I_p \sim v^1$ to $I_p \sim v^{0.5}$) at $v_{trans}=0.2$ Vs^{-1} (very approximately). From this transition scan rate, an estimate for the apparent diffusion coefficient of charge transport in the nano-composite can be obtained when considering the transition from linear to square root dependence of peak current on scan rate [41]. Here the apparent diffusion coefficient is estimated as $D_{app} = \frac{v_{trans}F}{RT}\left(\frac{\delta}{1.784}\right)^2 = 6 \times 10^{-14} m^2 s^{-1}$ (with a film thickness δ=160 nm, F the Faraday constant, R the gas constant, T=293 K). This over-simplistic analysis ignores possible complications from more complex transport effects such as percolation of a conducting emeraldine phase (vide infra), but it can provide an initial insight into the redox state switching rate in polyaniline–nanocellulose films.

Electrochemical characterisation of layer-by-layer polyaniline–nanocellulose composite films II.: nanogap generator–collector processes

In order to gain more quantitative experimental data additional experiments with an ITO junction electrode were conducted. Figure 4a shows the ITO pattern with the 700 nm gap (see SEM image in Fig. 4b) machined into the active part of the electrode. Polyaniline–nanocellulose films were deposited directly onto this junction and experiments were then performed with a bipotentiostat.

Figure 4c shows a typical cyclic voltammogram for a five-layer polyaniline–nanocellulose film immersed in aqueous 0.5 M H_2SO_4. Both sides of the electrode, generator and collector, are connected to the scanning generator potential (they are short-circuited). The resulting voltammetric response corresponds to the exposed polyaniline–nanocellulose film on both electrodes. Figure 4d shows the voltammogram obtained when the collector electrode is disconnected and only the generator electrode is connected. Perhaps surprisingly, the charge under the oxidation and reduction peaks is almost identical to that observed in Fig. 4c (that is, the currents did not half and electrical conductivity across the gap appears to connect the two electrodes). The appearance of a small intermediate peak (ca. 0.45 V vs. SCE) indicates the point where the junction becomes conducting due to the high electrical conductivity of the polyaniline–nanocellulose film. This effect is observed even more dramatically when the collector electrode is maintained at a fixed potential of −0.5 V

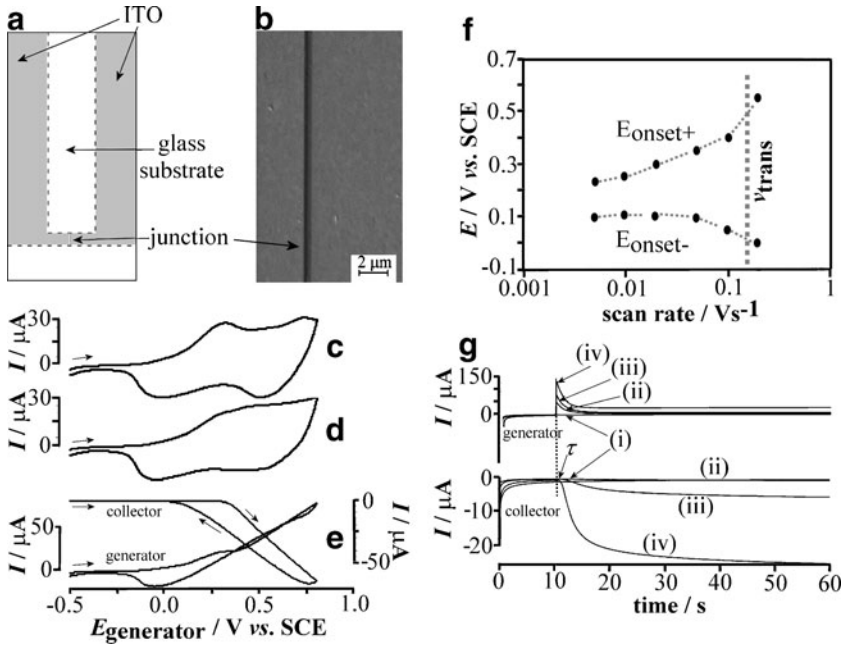

Fig. 4 **a** Schematic drawing of glass substrate with ITO coating patterned to give a small junction (cut by FIB). **b** SEM image of the cut in the ITO layer with ca. 700 nm width. **c** Cyclic voltammogram (scan rate 50 mVs^{-1}) for a five-layer polyaniline–nanocellulose film deposit on an ITO junction with both sides connected as working electrode. **d** As before, but with one side connected and the other disconnected. **e** As before, but generator–collector cyclic voltammogram data with the generator potential cycled from −0.5 to +0.8 V vs. SCE and the collector potential fixed at −0.5 V vs. SCE. **f** Plot of the onset potentials for the collector current as a function of scan rate. **g** Generator–collector chronoamperometry experiment with the collector potential fixed at −0.5 V vs. SCE and the generator potential stepped from −0.5 V vs. SCE to (*i*) 0.1, (*ii*) 0.2, (*iii*) 0.3 and (*iv*) 0.4 V vs. SCE

vs. SCE. Figure 4e shows the resulting generator and collector voltammetric responses. At approximately 0.4 V vs. SCE, the generator current response becomes strongly distorted because of additional current flowing between generator and collector. The magnitude of this current is limited by "Ohmic behaviour" with an approximate resistance of ca. 7 kOhm (estimated from the slope, consistent with the ITO film resistance for this device, and therefore consistent with high electrical conductivity in the polyaniline–nanocellulose film). By analysing the onset for the collector current for the scan in positive and in negative potential direction (E_{onset+} and E_{onset-}, respectively), more information can be obtained. The plot in Fig. 4f shows that the onset potentials are close to constant at a scan rate of less than 0.01 Vs^{-1} and they are rapidly diverging at scan rates higher than 0.1 or 0.2 Vs^{-1}. The transition point is again approximately 0.2 Vs^{-1} and therefore consistent with the behaviour of the peak current (vide supra). When assuming diffusional transport [42], the time required for the charge to propagate across the 700 nm junction can be estimated from $\tau = \delta^2/2D = 4s$ (with δ=700 nm and $D=6\times10^{-14}$ m^2s^{-1}). The actual onset point of the current across the junction occurs somewhat earlier (ca. 0.3 s) when observed in chronoamperometry experiments (see Fig. 4g), but the point of reaching half of the limiting current is in good agreement with the propagation time 3–4 s. Experiments with 10-layer polyaniline–nanocellulose and thicker films gave similar results. Literature reports on the mechanism of the polyaniline oxidation suggest more complex nucleation–growth processes during the formation

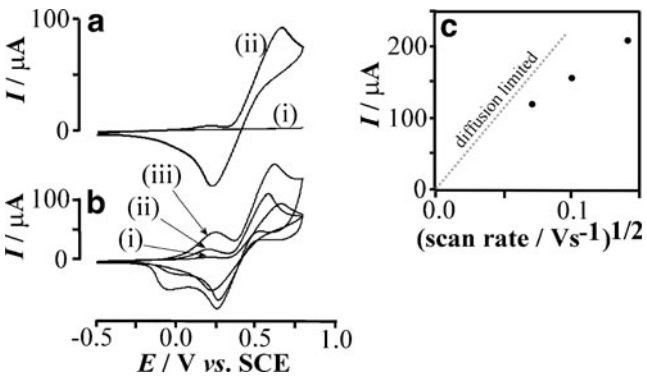

Fig. 5 **a** Cyclic voltammograms (scan rate 10 mVs^{-1}) for the oxidation of 1 mM hydroquinone in aqueous 0.1 M H_2SO_4 (*i*) at a bare ITO electrode and (*ii*) at a two-layer polyaniline–nanocellulose film electrode. **b** Cyclic voltammograms (scan rate 10 mVs^{-1}) for the oxidation of 1 mM hydroquinone in aqueous 0.1 M H_2SO_4 (*i*) at a two-layer, (*ii*) a five-layer and (*iii*) at a 10-layer polyaniline–nanocellulose film electrode **c** Plot of the anodic peak current for the oxidation of 1 mM hydroquinone in 0.1 M H_2SO_4 as a function of the square root of scan rate for a 10-layer polyaniline–nanocellulose film. The *dashed grey line* indicates the theoretical diffusion limited peak current assuming $D=0.86\times10^{-9}$ m^2s^{-1} for hydroquinone [48]

of the electrically conducting emeraldine phase [43]. In work by Aoki, the propagation rate of the conducting emeraldine phase was investigated [44] and shown to be potential dependent. For an applied potential of 0.4 V vs. SCE, a propagation rate of ca. 30 μm s^{-1} was observed and this corresponds to τ=23 μs for δ=700 nm. Comparison with the value obtained in this study, this suggests that the pure polyaniline film is switching approximately two orders of magnitude faster compared to the polyaniline–nanocellulose film. There are two important conclusions from this observation: (1) the electrically conducting emeraldine phase is formed even when a low content of polyaniline distributed in pores between cellulose fibrils is present and (2) electrical phenomena such as the propagation rate can be "tuned" based on the polyaniline content and the nanoarchitecture. The use of higher molecular weight polyaniline and/or triple-layer nanoarchitectures with a poly-cationic building block could be used to systematically change the electrical properties of polyaniline–nanocellulose films.

Electrochemical characterisation of layer-by-layer polyaniline–nanocellulose composite films III.: electrocatalysis

Films of polyaniline have been reported to show electro-catalyic effects in a range of applications [45] and as a particular example in the oxidation of hydroquinone [46, 47]. It is shown here that the polyaniline–nanocellulose film deposits exhibit similar catalytic activity. Figure 5a shows the oxidation of 1 mM hydroquinone in 0.5 M H_2SO_4 and (1) a bare ITO electrode and (2) a two-layer polyaniline–nanocellulose-modified ITO electrode. All redox activity is clearly linked to the presence of polyaniline catalyst.

In order to explore the electrocatalytic effect in more detail, the effect of the film thickness was investigated. Figure 5b shows cyclic voltammograms for the oxidation of 1 mM hydroquinone at a (1) two-layer, (2) five-layer and (3) 10-layer plolyaniline—nanocellulose electrode and the current enhancing effect in the thicker films is clearly observed. The voltammetric "pre-wave" at ca. 0.13 V vs. SCE can be identified as the polyaniline–nanocellulose oxidation process P1. The effect of the scan rate on the peak current for a 10-layer film is shown in Fig. 5c. The dotted line shows the anticipated peak current calculated based on the Randles-Sevcik equation [49] $I_p = 0.4463nF\left(\frac{nF}{RT}\right)^{1/2} c_{\text{bulk}} D^{1/2} v^{1/2}$ (with n=2, F the Faraday constant, R the gas constant, T=293 K, c_{bulk}=1 mol m^{-3} and $D=0.86\times10^{-9}$ m^2s^{-1} for hydroquinone) [48]. As expected the peak current does converge to the diffusion controlled limit for lower scan rates and for thicker polyaniline–nanocellulose films. For higher scan rates the underlying polyaniline response could affect the data, but in the case considered here the extrapolation to lower scan rates as employed is reliable. Voltammetric peak responses are directly proportional to the hydroquinone concentration.

Conclusion

Films of a polyaniline–nanocellulose composite are readily formed in a layer-by-layer electrostatic deposition process. Each layer is adding colour and causing an increase in average thickness of ca. 4 nm. Results from electrochemical measurements reflect the increase in thickness and are consistent with classical polyaniline redox processes. The predominant role of the nanocellulose is as a backbone in the composite film with polyaniline polymer dispersed as a linker. A switch in electrical conductivity has been observed with an ITO nanogap junction electrode and a time scale for propagation of the charge across the junction gap is suggested. When compared to pure polyaniline, the switching or propagation rate in polyaniline–nanocellulose is reduced consistent with a "nanoarchitecture" effect. Further work will be required for the full (e.g. numerical simulation) analysis of the nanogap junction voltammetry data and for further insight into and improvements in the nanoarchitecture-dependent electrical conductivity changes during redox state switching of polyaniline–nanocellulose films.

Acknowledgements Sara Shariki would like to thank Gharib Shariki and Maryam Shirmardi for financial support for this work. S.Y.L. thanks the University of Nottingham for a "Dean of Engineering International Research Scholarship" and the University of Nottingham Graduate School for a "Building Experience and Skills Travel Scholarship". Dr. Suguo Huo and Dr. Paul Warburton are gratefully acknowledged for allowing access to the EPSRC FIB service at UCL.

References

1. Wertz JL, Mercier JP, Bédué O (2010) Cellulose science and technology. EFPL, Lausanne
2. Macdiarmid AG, Epstein AJ (1995) Synth Metals 69:85
3. Liu P, Zhang L (2009) Crit Rev Solid State Mater Sci 34:75
4. Kim SH, Oh KW, Choi JH (2010) J Appl Polym Sci 116:2601
5. Houlton A, Pike AR, Galindo MA, Horrocks BR (2009) Chem Commun 14:1797–1806
6. Tran HD, Li D, Kaner RB (2009) Adv Mater 21:1487
7. Kang ET, Neoh KG, Tan KL (1998) Prog Polym Sci 23:277
8. Negi YS, Adhyapak PV (2002) J Macromol Sci Polym Rev C42:35
9. Wallace GG, Teasdale PR, Spinks GM, Kane-Maguire LAP (2008) Conductive electroactive polymers. CRC, New York
10. Greef R, Kalaji M, Peter LM (1989) Farad Disc 88:277
11. Tanami G, Gutkin V, Mandler D (2010) Langmuir 26:4239
12. Abu YM, Aoki K (2005) Electrochim Acta 50:3634
13. DeLongchamp DM, Hammond PT (2005) In: Jenekhe SA, Kiserow DJ (eds) Chromogenic phenomena in polymers—tunable optical properties. ACS Symp. Ser. 888:18
14. Žic M (2009) J Electroanal Chem 635:29

15. Krinichnyi VI, Tokarev SV, Roth HK, Schrodner M, Wessling B (2005) Synth Metals 152:165
16. Mo ZL, Zhao ZL, Chen H, Niu GP, Shi HF (2009) Carbohydrate Polym 75:660
17. Paakko M, Vapaavuori J, Silvennoinen R, Kosonen H, Ankerfors M, Lindstrom T, Berglund LA, Ikkala O (2008) Soft Matter 4:2492
18. van den Berg O, Schroeter M, Capadona JR, Weder C (2007) J Mater Chem 17:2746
19. John A, Mahadeva SK, Kim J (2010) Smart Mater Struct 19:045011/1
20. Lin DS, Chou CT, Chen YW, Kuo KT, Yang SM (2006) J Appl Polym Sci 100:4023
21. Mattoso LHC, Medeiros ES, Baker DA, Avloni J, Wood DF, Orts WJ (2009) J Nanosci Nanotechnol 9:2917
22. Decher G, Schlenoff J (Eds) (2003) Multilayer Thin Films: Sequential Assembly of Nanocomposite Materials, Wiley–VCH, Weinheim
23. Castelnovo M, Joanny JF (2000) Langmuir 16:7524
24. Klemm D, Heublein B, Fink HP, Bohn A (2005) Angew Chem Intern Ed 44:3358
25. Habibi Y, Lucia LA, Rojas OJ (2010) Chem Rev 110:3479
26. Aulin C, Johansson E, Wagberg L, Lindstrom T (2010) Biomacromol 11:872
27. de Mesquita JP, Donnici CL, Pereira FV (2010) Biomacromol 11:473
28. Liew SY, Thielemans W, Walsh DA (2010) J Phys Chem C 114:17926
29. Jean B, Dubreuil F, Heux L, Cousin F (2008) Langmuir 24:3452
30. Zhao Q, Qian JW, An QF, Sun ZW (2010) J Membrane Sci 346:335
31. Bonné MJ, Milsom EV, Helton M, Thielemans W, Wilkins S, Marken F (2007) Electrochem Commun 9:1985
32. Medeiros ES, Mattoso LHC, Bernardes-Filho R, Wood DF, Orts WJ (2008) Coll Polym Sci 286:1265
33. de Rodriguez NLG, Thielemans W, Dufresne A (2006) Cellulose 13:261
34. DeLongchamp DM, Hammond PT (2004) Chem Mater 16:4799
35. John A, Mahadeva SK, Kim J (2010) Smart Mater Struct 19:045011
36. Tsai TH, Wu YF (2006) J Electrochem Soc 153:C86
37. Kuila BK, Stamm M (2010) J Mater Chem 20:6086
38. Huang WS, Macdiarmid AG (1993) Polym 34:1833
39. Farag AAM, Ashery A, Rafea MA (2010) Synth Metals 160:156
40. Bonné MJ, Galbraith E, James TD, Wasbrough MJ, Edler KJ, Jenkins ATA, Helton M, McKee A, Thielemans W, Psillakis E, Marken F (2010) J Mater Chem 20:588
41. Milsom EV, Novak J, Green SJ, Zhang XH, Stott SJ, Mortimer RJ, Edler K, Marken F (2007) J Solid State Electrochem 11:1109
42. Atkins PW (2006) Physical chemistry, 8th edn. Oxford University Press, Oxford, 781
43. Kalaji M, Nyholm L, Peter LM (1992) J Electroanal Chem 325:269
44. Aoki K, Kawase M (1994) J Electroanal Chem 377:125
45. Malinauskas A (1999) Synth Metals 107:75
46. Buttner E, Holze R (2001) J Electroanal Chem 508:150
47. Duic L, Grigic S (2001) Electrochim Acta 46:2795
48. Adams RN (1969) Electrochemistry at solid electrodes. Marcel Dekker, New York, p221
49. Group SE (2001) Instrumental methods in electrochemistry. Horwood Publishing, Chichester, 183